

# Quantum Phase Transitions in Coherent Ising Machines: XY Model for Demonstration

Jing-Yi-Ran Jin,<sup>1,2</sup> Shuang-Quan Ma,<sup>1,2</sup> and Qing Ai<sup>1,2,\*</sup>

<sup>1</sup>*School of Physics and Astronomy, Applied Optics Beijing Area Major Laboratory, Beijing Normal University, Beijing 100875, China*

<sup>2</sup>*Key Laboratory of Multiscale Spin Physics, Ministry of Education, Beijing Normal University, Beijing 100875, China*

Quantum phase transitions (QPTs) in coherent Ising machines (CIMs) are studied via a spectral mapping between the one-dimensional XY spin model and a network of degenerate optical parametric oscillators (DOPOs). This exact correspondence reveals that the DOPO network faithfully reproduces the quantum critical behavior of the XY model across its anisotropic, isotropic, and transverse-field Ising regimes. The ground-state energy density and its derivatives are analyzed to reveal second-order QPTs characterized by singularities in magnetic susceptibility at critical points. These results show that CIMs do not only serve as powerful platforms for solving combinatorial optimization problems but also provide a versatile optical simulator for studying universal quantum critical phenomena, bridging quantum-spin models and photonic quantum systems.

## I. INTRODUCTION

Quantum phase transitions (QPTs) mark fundamental changes in the ground state of a quantum many-body system, driven solely by quantum fluctuations at zero temperature. Unlike classical phase transitions, which arise from thermal fluctuations, QPTs occur when a control parameter (e.g., magnetic field or coupling strength) in the systems Hamiltonian is tuned across a critical point, leading to non-analytic behavior in the ground-state energy. This abrupt change reflects a reorganization of quantum correlations and often accompanies the closing of the energy gap in the thermodynamic limit [1, 2]. The study of QPTs does not only illuminate the deep structure of quantum matter [3–8] but also bridges seemingly disparate fields such as condensed matter physics [9–13], quantum information science [14–17], and critical phenomena [18–21]. In particular, the enhanced quantum fluctuations and long-range entanglement near critical points offer novel mechanisms for quantum sensing [22–26], topological materials [27–29], and the engineering of exotic phases of matter [30–32]. As such, QPTs serve as both a theoretical cornerstone and a practical frontier in the exploration of strongly correlated quantum systems.

Building upon the theoretical framework of QPTs, the one-dimensional XY model provides an analytically accessible yet physically rich platform for exploring quantum critical phenomena [33–40]. The model captures essential features of quantum magnetism, such as competition between exchange interactions and external fields, while remaining exactly solvable. This solvability therefore enables the precise identification of quantum critical points, which are characterized by the closing of the energy gap and the emergence of universal

scaling behavior. This universality likewise makes it a useful model for investigating quantum battery [41, 42] and quantum discord [43–45].

Experimentally, the quantum critical phenomena of the XY model can be accessed through the coherent Ising machine (CIM), which bridges its theoretical description with a tunable physical implementation. At its core, a CIM employs degenerate optical parametric oscillators (DOPOs) to simulate qubits, enabling efficient computation of the ground state. When the pump intensity surpasses the bifurcation threshold, the system undergoes a collective spontaneous symmetry breaking, driving it from the normal phase to the superradiant phase [46, 47]. Originally harnessed for solving Ising-based optimization problems [48–52], the nonlinear and collective dynamics of DOPO networks have since established CIMs as versatile simulators for quantum many-body phenomena, including phase transitions [53–56]. Beyond physics simulation, they are also used in many fields such as chemical synthesis [57, 58] and biology [59].

Following this introduction, the paper is organized as follows. In Sec. II, we introduce the XY spin model and the DOPO network, and establish the spectral mapping between them. In Sec. III, we present numerical results for the ground-state energy density and its derivatives, and discuss the simulated QPT. We conclude in Sec. IV and provide an outlook on future directions.

## II. MODEL

### A. XY Model

The XY model represents a fundamental quantum spin system that exhibits rich critical behavior [1]. With  $\hbar =$

\* [aiqing@bnu.edu.cn](mailto:aiqing@bnu.edu.cn)

1, the Hamiltonian for this model is given by

$$H_{XY} = - \sum_{i=1}^{N-1} (J_x \sigma_i^x \sigma_{i+1}^x + J_y \sigma_i^y \sigma_{i+1}^y) - h \sum_{i=1}^N \sigma_i^z, \quad (1)$$

where  $J_x$  ( $J_y$ ) denote the coupling strength along the  $x$  ( $y$ ) direction,  $h$  represents the transverse field, and  $\sigma_i^\alpha$  ( $\alpha = x, y, z$ ) are the Pauli matrices.

To analyze this system, we first employ the Jordan-Wigner transformation [1] to map the spin operators to the fermionic operators as

$$\begin{aligned} \sigma_i^+ &= c_i^\dagger e^{i\pi \sum_{j=1}^{i-1} c_j^\dagger c_j}, \\ \sigma_i^- &= c_i e^{i\pi \sum_{j=1}^{i-1} c_j^\dagger c_j}, \\ \sigma_i^z &= 2c_i^\dagger c_i - 1. \end{aligned} \quad (2)$$

Here  $\sigma_i^+$  and  $\sigma_i^-$  denote the raising and lowering operators for the  $i$ th spin, defined as  $\sigma_i^\pm = (\sigma_i^x \pm i\sigma_i^y)/2$ .  $c_i^\dagger$  ( $c_i$ ) is the fermionic creation (annihilation) operator satisfying  $\{c_i, c_j^\dagger\} = \delta_{ij}$ . Transforming to momentum space under periodic boundary conditions, with  $c_i = \sum_k e^{ikx_i} c_k / \sqrt{N}$  and  $k = 2\pi m/N$  ( $m = -N/2 + 1, \dots, N/2$ ), the Hamiltonian becomes

$$\begin{aligned} H'_{XY} = & - \sum_k \{i(J_x - J_y) \sin k (c_k^\dagger c_{-k}^\dagger + c_k c_{-k}) \\ & + 2[(J_x + J_y) \cos k + h] c_k^\dagger c_k\} + hN. \end{aligned} \quad (3)$$

After performing the Bogoliubov transformation [1], we can diagonalize the Hamiltonian as

$$H'_{XY} = \sum_k E_k^{XY} \gamma_k^\dagger \gamma_k + E_0^{XY}, \quad (4)$$

in which  $\gamma_k^\dagger$  ( $\gamma_k$ ) represent the Bogoliubov quasiparticle creation (annihilation) operators. The corresponding energy spectrum and ground-state energy are

$$E_k^{XY} = 2\sqrt{[h + (J_x + J_y) \cos k]^2 + [(J_x - J_y) \sin k]^2}, \quad (5)$$

$$E_0^{XY} = -\frac{1}{2} \sum_k E_k, \quad (6)$$

respectively.

In the thermodynamic limit, i.e.,  $N \rightarrow \infty$ , the energy density of the ground state becomes

$$e_g^{XY} = \lim_{N \rightarrow \infty} \frac{E_0^{XY}}{N} = -\frac{1}{2\pi} \int_0^\pi E_k^{XY} dk. \quad (7)$$

The critical points where the QPT occurs can be identified by examining the closure of the energy gap, i.e.,  $\min_k(E_k) = 0$ . This leads to the conditions, i.e.,

$$\begin{aligned} h + (J_x + J_y) \cos k &= 0, \\ (J_x - J_y) \sin k &= 0, \end{aligned} \quad (8)$$

which should be satisfied simultaneously. This analysis reveals several important cases, which will be illustrated in the following subsections.

### 1. Isotropic XY Model with $J_x = J_y = J$

For the isotropic case, the condition (8) is simplified as

$$h + 2J \cos k = 0. \quad (9)$$

The critical points occur at  $h_c = \pm 2J$ , as  $\cos k \in [-1, 1]$ . This symmetric behavior reflects the rotational invariance of the isotropic model.

### 2. Anisotropic XY Model with $J_x \neq J_y$

In the general case with anisotropic couplings, the condition (8) requires  $\sin k = 0$ , i.e.,  $k = 0$  or  $k = \pi$ , leading to the critical fields as

$$\begin{aligned} h_c &= -(J_x + J_y), \quad \text{for } k = 0, \\ h_c &= J_x + J_y, \quad \text{for } k = \pi. \end{aligned} \quad (10)$$

The critical behavior thus depends on the sum of the two coupling constants.

### 3. TFI model with $J_y = 0$ and $J_x = J > 0$

This important special case yields

$$\begin{aligned} h_c &= -J, \quad \text{for } k = 0, \\ h_c &= J, \quad \text{for } k = \pi. \end{aligned} \quad (11)$$

For simplicity, we adopt the convention of a positive transverse field  $h > 0$  throughout this work. Under this convention, the QPT driven by increasing  $h$  from zero occurs at the critical field  $h_c = J_x + J_y$ , which corresponds to the gap closing at momentum  $k = \pi$  as given in Eq. (10). This marks the transition from a ferromagnetically ordered phase to a paramagnetic phase. The alternative critical point  $h_c = -(J_x + J_y)$  for  $k = 0$  corresponds to a negative transverse field; it is physically equivalent to the positive-field case under a global spin rotation (e.g., a  $\pi$  rotation around the  $x$ -axis flips the sign of  $h$ ).

## B. Network of $N$ -DOPOs

In a DOPO with second-order nonlinear effects, a pump field at frequency  $\omega_p$  undergoes parametric down-conversion within the nonlinear medium, yielding a signal field with frequency  $\omega_s$  and an idler field with frequency  $\omega_i$ . As illustrated in Fig. 1 (a), the Hamiltonian of the system can be expressed as

$$H_D = H_0 + H_{\text{int}}, \quad (12)$$

where

$$H_0 = \omega_s a_s^\dagger a_s + \omega_p a_p^\dagger a_p, \quad (13)$$

$$H_{\text{int}} = i\frac{\kappa}{2} a_s^{\dagger 2} a_p + i\varepsilon a_p^\dagger e^{-i\omega_p t} + \text{H.c.} \quad (14)$$

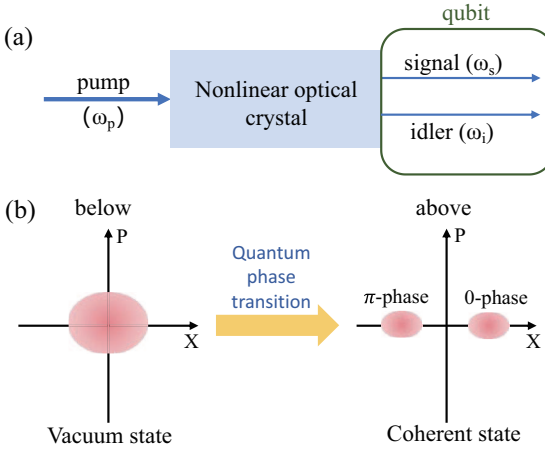


FIG. 1. (a) Schematic representation of a DOPO, a key component for constructing a CIM. (b) Simplified phase-space illustration of a DOPO: the vacuum state below the threshold and the coherent state corresponding to phases 0 and  $\pi$  above the threshold.

Here  $a_s^\dagger$  ( $a_s$ ) and  $a_p^\dagger$  ( $a_p$ ) are the creation (annihilation) operators for the signal and pump fields, respectively. The coupling constant  $\kappa$  quantifies the strength of the second-order nonlinear interaction, and  $\varepsilon$  is the amplitude of the external coherent drive applied to the pump mode. When there is a detuning  $\Delta = \omega_s - (\omega_p/2)$  between the signal and the pump fields, with respect to the free Hamiltonian

$$H_f = \frac{\omega_p}{2} a_s^\dagger a_s + \omega_p a_p^\dagger a_p, \quad (15)$$

the Hamiltonians are transformed to the interaction picture as

$$H'_0 = \Delta a_s^\dagger a_s, \quad (16)$$

$$H'_{\text{int}} = i \frac{\kappa}{2} a_s^{\dagger 2} a_p e^{2i\Delta t} + i \varepsilon a_p^\dagger + \text{H.c.} \quad (17)$$

Following the Heisenberg-Langevin approach [60], the temporal evolution of the pump field is described by

$$\frac{da_p}{dt} = -\gamma_p a_p + \varepsilon - \frac{\kappa}{2} a_s^2 e^{-2i\Delta t}, \quad (18)$$

where  $\gamma_p$  represents the decay rate of the pump mode. Assuming the pump field reaches its steady state rapidly, we adiabatically eliminate it to obtain an effective Hamiltonian for the signal mode as

$$H_D = \Delta a^\dagger a + i \frac{\kappa \varepsilon}{2\gamma_p} a^{\dagger 2} + \text{H.c.} \quad (19)$$

Hereafter, we omit the subscript  $s$  for the signal field for simplicity.

Extending this description to  $N$  nearest-neighbor-coupled DOPOs yields the generalized Hamiltonian

$$H_{\text{ND}} = \sum_{i=1}^N \Delta \hat{a}_i^\dagger \hat{a}_i + \sum_{i=1}^N \left( i \frac{\kappa \varepsilon}{2\gamma_p} \hat{a}_i^{\dagger 2} - J \hat{a}_i^\dagger \hat{a}_{i+1} \right) + \text{H.c.}, \quad (20)$$

where  $\hat{a}_i^\dagger$  ( $\hat{a}_i$ ) is the creation (annihilation) operator for the  $i$ th DOPO, and  $J$  quantifies the coupling strength between two adjacent DOPOs. To diagonalize  $H_{\text{ND}}$ , we first move to momentum space via a Fourier transformation, which brings the Hamiltonian into the form

$$H'_{\text{ND}} = \sum_k \left( \epsilon_k \hat{a}_k^\dagger \hat{a}_k + i \frac{\kappa \varepsilon}{2\gamma_p} \hat{a}_k^\dagger \hat{a}_{-k}^\dagger + \text{H.c.} \right), \quad (21)$$

where we have defined  $\epsilon_k = \Delta - 2J \cos k$  for brevity. A subsequent Bogoliubov transformation

$$\hat{b}_k = \hat{a}_k \cosh r_k + \hat{a}_{-k}^\dagger e^{i\theta} \sinh r_k \quad (22)$$

is then applied, where the parameters are chosen as  $\tanh(2r_k) = |\kappa \varepsilon|/(\gamma_p \epsilon_k)$  and  $\theta = \arg(\kappa \varepsilon) + \pi/2$  to remove off-diagonal terms. The resulting diagonal Hamiltonian is

$$H'_{\text{ND}} = \sum_k \Omega_k \hat{b}_k^\dagger \hat{b}_k + \frac{1}{2} \sum_k (\Omega_k - \epsilon_k), \quad (23)$$

where the quasiparticle energy spectrum reads

$$\Omega_k = \sqrt{\epsilon_k^2 - \left| \frac{\kappa \varepsilon}{\gamma_p} \right|^2}, \quad (24)$$

and the second sum corresponds to the zero-point energy contribution.

In this framework, the DOPO network exhibits a QPT from a normal phase (vacuum state) to a superradiant phase (coherent state) when the pump intensity exceeds the threshold, as shown in Fig. 1(b). This optical symmetry-breaking transition is mathematically analogous to the ferromagnetic-to-paramagnetic transition in the XY model, despite their distinct physical origins.

### C. Energy-Spectrum Matching

We now present a rigorous mapping between the energy spectra of the XY model and that of the  $N$ -DOPO network. Defining  $J_s = J_x + J_y$ ,  $J_d = J_x - J_y$ , and  $D = |\kappa \varepsilon / \gamma_p|$ , the squared energy spectrum of the XY model is given by

$$(E_k^{\text{XY}})^2 = 4(h^2 + J_d^2) + 8J_s h \cos k + 16J_x J_y \cos^2 k. \quad (25)$$

Meanwhile, the squared energy spectrum of the DOPO network reads

$$\Omega_k^2 = \Delta^2 - D^2 - 4\Delta J \cos k + 4J^2 \cos^2 k. \quad (26)$$

Requiring the two spectra to coincide for all  $k$ , we obtain the exact mapping

$$\begin{aligned} J &= 2\sqrt{J_x J_y}, \\ \Delta &= -\frac{h J_s}{\sqrt{J_x J_y}}, \\ D^2 &= J_d^2 \left( \frac{h^2}{J_x J_y} - 4 \right). \end{aligned} \quad (27)$$

Through this transformation, the critical behavior of the XY model can be faithfully studied in the DOPO network. In the thermodynamic limit, the energy density satisfies

$$e_g^D = -e_g^{XY} + \frac{hJ_s}{2\sqrt{J_x J_y}}. \quad (28)$$

This relationship implies that the non-analyticities in the ground-state energy of the XY model, which characterize the QPT, are directly inherited by the DOPO network, albeit with a linear shift and scaling.

### III. RESULTS AND DISCUSSION

As illustrated in Fig. 2, we consider three quantum spin-chain models: the anisotropic XY model with parameters  $J_x = 2$  and  $J_y = 1$ , the isotropic XY model with  $J_x = J_y = 1$ , and the TFI model with  $J_x = 1$  and  $J_y = 0$ . Each model exhibits a second-order QPT driven by the transverse magnetic field  $h$ . In the absence of the field ( $h = 0$ ), the TFI model and the anisotropic XY model (where  $J_x > J_y$ ) exhibit spontaneous ordering, characterized by a non-zero magnetization  $m_x$ , while  $m_y = m_z = 0$ . In contrast, the isotropic XY model retains full rotational symmetry within the  $x$ - $y$  plane, leading to  $m_x = m_y = m_z = 0$  at zero field. As  $h$  increases from zero, the ground-state energy density  $e_g^{XY}$  and the longitudinal magnetization  $m_z^{XY}$  evolve continuously. At the critical field strength  $h_c = J_x + J_y$ , each system undergoes a QPT into a paramagnetic phase, where the spins become predominantly aligned along the field direction. For  $h > h_c$ , the longitudinal magnetization  $m_z$  increases monotonically toward its saturation value of +1, whereas the transverse components  $m_x$  and  $m_y$  are suppressed to zero. The magnetic susceptibility  $\chi^{XY}$  displays a divergence near  $h_c$ , directly signaling the critical point. For the isotropic XY model in the paramagnetic phase, the first derivative of the ground-state energy density remains constant, leading to a vanishing second derivative. This accounts for the disappearance of its corresponding curve beyond  $h_c$  in the logarithmic-scale plot of Fig. 2(c). Collectively, this systematic analysis provides a clear physical interpretation and numerical verification for the simulation of quantum critical phenomena using a CIM.

The simulated ground-state properties of the DOPO network are presented in Fig. 3. The three columns correspond to different regimes of the XY model mapped onto the optical system. The left column, with parameters  $J = 2\sqrt{2}$  and  $\Delta = -3h/\sqrt{2}$ , represents the

anisotropic XY model. The middle column, with  $J = 2$ ,  $\Delta = -2h$ , and  $D = 0$ , corresponds to the isotropic XY model. The right column approximates the TFI limit using a strongly anisotropic XY model with  $J_y \ll J_x$ . For concreteness, taking  $J_x = 1$  and  $J_y = 0.01$ , the mapping in Eq. (27) gives  $J = 0.2$  and  $\Delta = -10h$ . The phase transition in all three cases occurs at  $\Delta_c = -2J - D$ , exhibiting the characteristic second-order QPT behavior seen in the spin chains. For  $\Delta < \Delta_c$ , the system is in the normal phase with a real excitation spectrum  $\Omega_k$ . When  $\Delta > \Delta_c$ , it enters the superradiant phase where the optical symmetry is spontaneously broken, and  $\Omega_k$  becomes imaginary for certain  $k$  modes, indicating dynamical instability. This consistent critical behavior demonstrates that the universal quantum criticality of the XY spin chain is faithfully reproduced in the DOPO network through the spectral mapping.

### IV. CONCLUSION

In this work, we have established a rigorous spectral mapping between the XY spin chain and a network of DOPOs, enabling the simulation of QPT in a CIM. We derive explicit relations between the parameters of the XY model and those of the DOPO network, demonstrating that critical behavior, including gap closure and non-analyticities in ground-state energy, is faithfully reproduced in the optical system. Numerical results for anisotropic, isotropic, and TFI models confirm that the DOPO network exhibits second-order QPTs consistent with those of the corresponding spin models, as evidenced by singularities in magnetic susceptibility and discontinuities in energy derivatives.

The ability to map spin Hamiltonians onto photonic networks opens new avenues for studying quantum criticality in tunable optical platforms, with potential applications in quantum sensing, quantum information, and the simulation of condensed-matter phenomena. Future work may extend this approach to higher-dimensional system, further exploring the interplay between optical nonlinearity and QPTs.

### V. ACKNOWLEDGMENTS.

This work is supported by the National Natural Science Foundation of China under Grant No. 62461160263, and Quantum Science and Technology-National Science and Technology Major Project (2023ZD0300200), and Guangdong Provincial Quantum Science Strategic Initiative under Grant No. GDZX2505004.

[1] S. Sachdev, *Quantum Phase Transitions*, 2nd ed. (Cambridge University Press, 2011).

[2] M.-J. Hwang, R. Puebla, and M. B. Plenio, “Quantum Phase Transition and Universal Dynamics in the Rabi

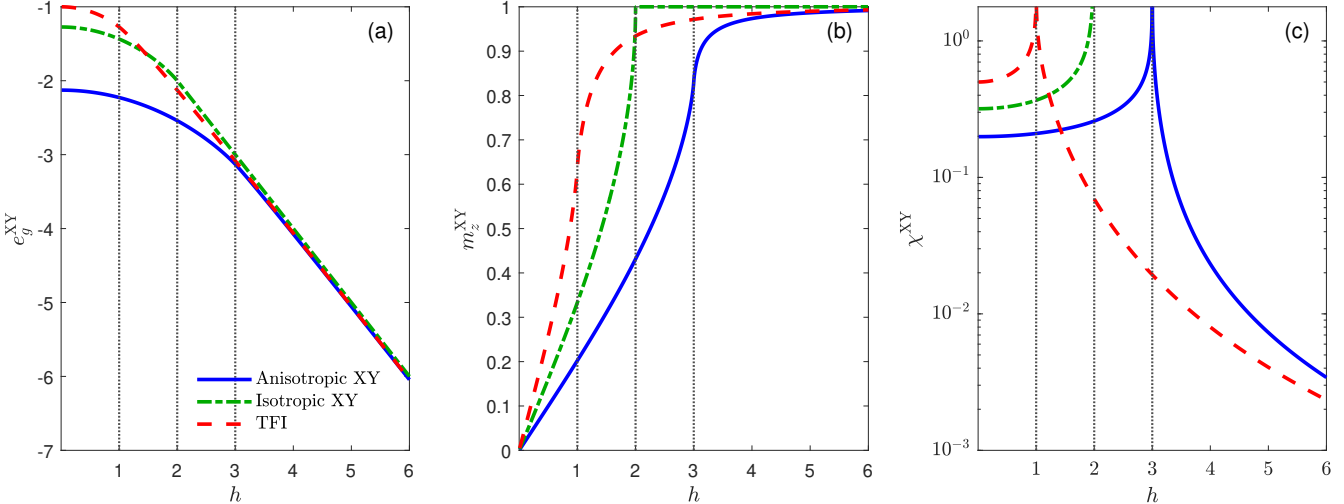


FIG. 2. Numerical results for three quantum-spin-chain models under an external field  $h$ : (a) Ground-state energy density  $e_g^{\text{XY}}$ , (b) magnetization  $m_z^{\text{XY}} = -\partial e_g^{\text{XY}} / \partial h$ , and (c) magnetic susceptibility  $\chi^{\text{XY}} = -\partial^2 e_g^{\text{XY}} / \partial h^2$ . Note that sub-figure (c) uses a logarithmic scale. The curves correspond to the anisotropic XY model ( $J_x = 2, J_y = 1$ , blue solid line), the isotropic XY model ( $J_x = J_y = 1$ , green dash-dotted line), and the transverse-field Ising model ( $J_x = 1, J_y = 0$ , red dashed line). The vertical dotted lines mark the calculated critical fields  $h_c$  for each model.

Model,” *Phys. Rev. Lett.* **115**, 180404 (2015).

- [3] T.-C. Hu, H.-Q. Pi, S.-X. Xu, L. Yue, Q. Wu, Q.-M. Liu, S.-J. Zhang, R.-S. Li, X.-Y. Zhou, J.-Y. Yuan, D. Wu, T. Dong, H.-M. Weng, and N.-L. Wang, “Optical spectroscopy and band structure calculations of the structural phase transition in the vanadium-based kagome metal  $\text{ScV}_6\text{Sn}_6$ ,” *Phys. Rev. B* **107**, 165119 (2023).
- [4] Z. Zhu, D. N. Sheng, and I. Sodemann, “Widely Tunable Quantum Phase Transition from Moore-Read to Composite Fermi Liquid in Bilayer Graphene,” *Phys. Rev. Lett.* **124**, 097604 (2020).
- [5] N. E. Myerson-Jain, S. Yan, D. Weld, and C.-K. Xu, “Construction of Fractal Order and Phase Transition with Rydberg Atoms,” *Phys. Rev. Lett.* **128**, 017601 (2022).
- [6] S. Arya, M. S. Laad, and S. R. Hassan, “Quantum phase transitions in strained graphene due to the interplay between spin fluctuations and anisotropic band structure,” *Phys. Rev. B* **96**, 085126 (2017).
- [7] Y.-P. Zhang, G. Chen, and C.-W. Zhang, “Tunable Spin-orbit Coupling and Quantum Phase Transition in a Trapped Bose-Einstein Condensate,” *Sci. Rep.* **3**, 1937 (2013).
- [8] J. Hertkorn, J.-N. Schmidt, F. Böttcher, M. Guo, M. Schmidt, K. S. H. Ng, S. D. Graham, H. P. Büchler, T. Langen, M. Zwierlein, and T. Pfau, “Density fluctuations across the superfluid-supersolid phase transition in a dipolar quantum gas,” *Phys. Rev. X* **11**, 011037 (2021).
- [9] N. Maksimovic, D. H. Eilbott, T. Cookmeyer, F.-H. Wan, J. Rusz, V. Nagarajan, S. C. Haley, E. Maniv, A. Gong, S. Faubel, I. M. Hayes, A. Bangura, J. Singleton, J. C. Palmstrom, L. Winter, R. McDonald, S. Y. Jang, Ping. Ai, Y. Lin, S. Ciocys, J. Gobbo, Y. Werman, P. M. Oppeneer, E. Altman, A. Lanzara, and J. G. Analytis, “Evidence for a delocalization quantum phase transition without symmetry breaking in  $\text{CeCoIn}5$ ,” *Science* **375**, 76 (2022).
- [10] W. Wang and Z.-S. Ma, “Real-complex quantum phase transition in non-hermitian disorder-free systems,” *Phys. Rev. B* **106**, 115306 (2022).
- [11] S. Bhattacharyya, S. Dasgupta, and A. Das, “Signature of a continuous quantum phase transition in non-equilibrium energy absorption: Footprints of criticality on higher excited states,” *Sci. Rep.* **5**, 16490 (2015).
- [12] Vipin Vijayan, L. Chotorlishvili, A. Ernst, S. S. P. Parkin, M. I. Katsnelson, and S. K. Mishra, “Topological dynamical quantum phase transition in a quantum skyrmion phase,” *Phys. Rev. B* **107**, L100419 (2023).
- [13] A. Paviglianiti and A. Silva, “Multipartite entanglement in the measurement-induced phase transition of the quantum Ising chain,” *Phys. Rev. B* **108**, 184302 (2023).
- [14] Y.-C. Zhang, L. Vidmar, and M. Rigol, “Information measures for a local quantum phase transition: Lattice fermions in a one-dimensional harmonic trap,” *Phys. Rev. A* **97**, 023605 (2018).
- [15] S. Sahu, S.-L. Xu, and B. Swingle, “Scrambling dynamics across a thermalization-localization quantum phase transition,” *Phys. Rev. Lett.* **123**, 165902 (2019).
- [16] M. Heyl, F. Pollmann, and B. Dóra, “Detecting Equilibrium and Dynamical Quantum Phase Transitions in Ising Chains via Out-of-Time-Ordered Correlators,” *Phys. Rev. Lett.* **121**, 016801 (2018).
- [17] Q. Ai, T. Shi, G.-L. Long, and C.-P. Sun, “Induced entanglement enhanced by quantum criticality,” *Phys. Rev. A* **78**, 022327 (2008).
- [18] E. Brillaux, A. A. Fedorenko, and I. A. Gruzberg, “Surface quantum critical phenomena in disordered Dirac semimetals,” *Phys. Rev. B* **109**, 174204 (2024).
- [19] Z. Wu, T. I. Weinberger, A. J. Hickey, D. V. Chichinadze, D. Shaffer, A. Cabala, H. Chen, M. Long, T. J. Brumm,

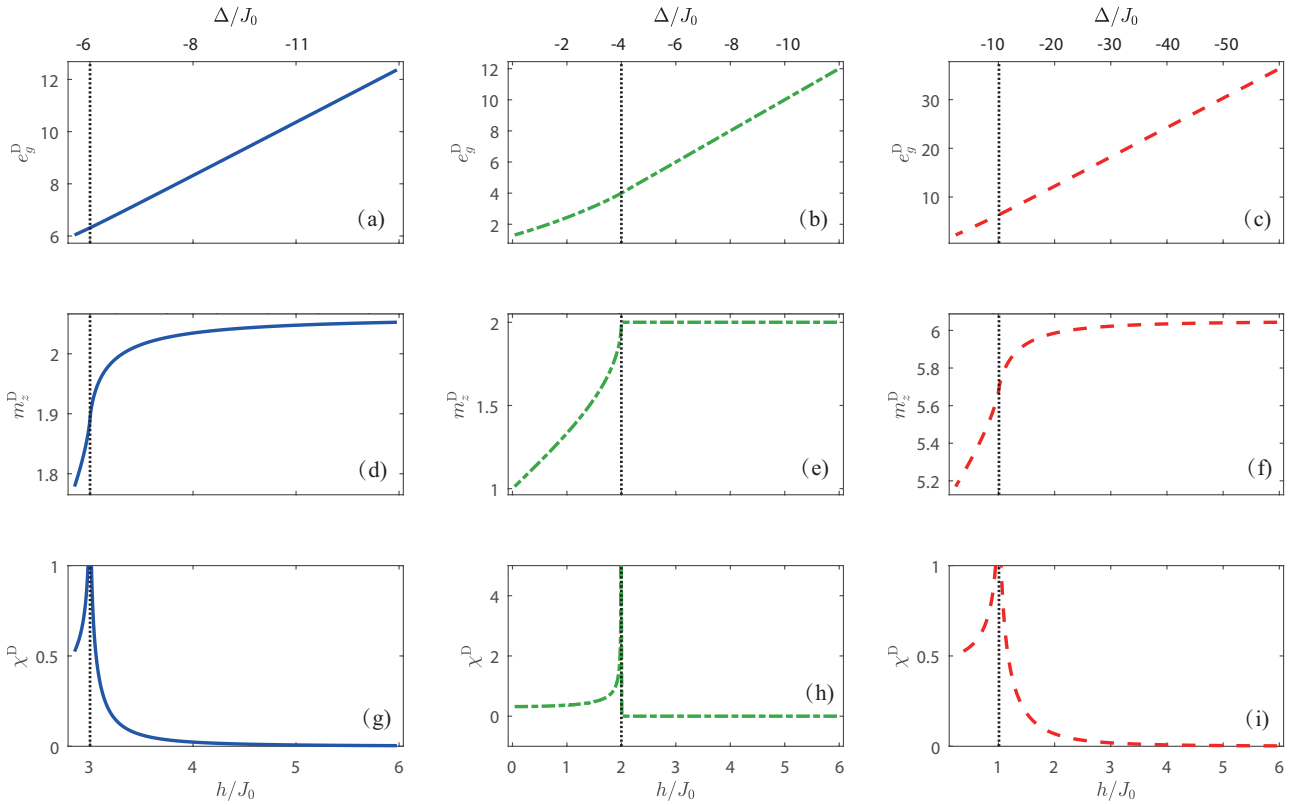


FIG. 3. QPTs in a DOPO network mapped from the XY model. Columns show DOPO parameter regimes: (left)  $J = 2\sqrt{2}$ ,  $\Delta = -3h/\sqrt{2}$ ; (middle)  $J = 2$ ,  $\Delta = -2h$  ( $D = 0$ ); (right)  $J = 0.2$ ,  $\Delta = -10h$ . These correspond to anisotropic XY, isotropic XY, and near-TFI spin chains, respectively. From top to bottom, the panels display: (a–c) the ground-state energy density  $e_g^D$ ; (d–f) the longitudinal magnetization  $m_z^D$ ; and (g–i) the magnetic susceptibility  $\chi^D$ . Each panel features dual horizontal axes: the upper axis shows the DOPO detuning parameter  $\Delta$ , and the lower axis shows the corresponding transverse field  $h$  in the XY model. All energies are scaled by  $J_0 = 1$  to render them dimensionless. Vertical dashed lines indicate the critical points at  $\Delta_c = -2J - D$ .

W. Xie, Y. Ling, Z. Zhu, Y. Skourski, D. E. Graf, V. Sechovský, M. Vališka, G. G. Lonzarich, F. M. Grosche, and A. G. Eaton, “A Quantum Critical Line Bounds the High Field Metamagnetic Transition Surface in  $\text{UTe}_2$ ,” *Phys. Rev. X* **15**, 021019 (2025).

[20] H. J. Kim, F. Gay, A. Del Maestro, B. Sacepe, and A. Rogachev, “Pair-breaking quantum phase transition in superconducting nanowires,” *Nat. Phys.* **14**, 912 (2018).

[21] W.-T. He, C.-W. Lu, Y.-X. Yao, H.-Y. Zhu, and Q. Ai, “Criticality-based quantum metrology in the presence of decoherence,” *Front. Phys.* **18**, 31304 (2023).

[22] S.-B. Tang, H. Qin, B.-B. Liu, D.-Y. Wang, K.-F. Cui, S.-L. Su, L.-L. Yan, and G. Chen, “Enhancement of quantum sensing in a cavity-optomechanical system around the quantum critical point,” *Phys. Rev. A* **108**, 053514 (2023).

[23] J.-H. Lü, W. Ning, X. Zhu, F. Wu, L.-T. Shen, Z.-B. Yang, and S.-B. Zheng, “Critical quantum sensing based on the Jaynes-Cummings model with a squeezing drive,” *Phys. Rev. A* **106**, 062616 (2022).

[24] L. Shao, R. Zhang, W.-J. Lu, Z.-C. Zhang, and X.-G. Wang, “Quantum phase transition in the  $XXZ$  central spin model,” *Phys. Rev. A* **107**, 013714 (2023).

[25] T. L. Heugel, M. Biondi, O. Zilberberg, and R. Chitra, “Quantum transducer using a parametric driven-dissipative phase transition,” *Phys. Rev. Lett.* **123**, 173601 (2019).

[26] Q. Guan and R. J. Lewis-Swan, “Identifying and harnessing dynamical phase transitions for quantum-enhanced sensing,” *Phys. Rev. Res.* **3**, 033199 (2021).

[27] M. Shafiei, F. Fazileh, F. M. Peeters, and M. V. Milošević, “Tuning the quantum phase transition of an ultrathin magnetic topological insulator,” *Phys. Rev. Mater.* **8**, 074201 (2024).

[28] H. Sun, S.-S. Li, W.-X. Ji, and C.-W. Zhang, “Valley-dependent topological phase transition and quantum anomalous valley Hall effect in single-layer  $\text{RuClBr}$ ,” *Phys. Rev. B* **105**, 195112 (2022).

[29] M. Mogi, D.-S. Choi, L. Primeau, B.-Q. Lv, D. Azoury, Y.-F. Su, L. Fu, Y. Zhang, and N. Gedik, “Direct observation of a photoinduced topological phase transition in Bi-Doped  $(\text{Pb},\text{Sn})\text{Se}$ ,” *Phys. Rev. Lett.* **133**, 236601 (2024).

[30] M. Kalinowski, R. Samajdar, R. G. Melko, M. D. Lukin, S. Sachdev, and S. W. Choi, “Bulk and boundary

quantum phase transitions in a square Rydberg atom array,” *Phys. Rev. B* **105**, 174417 (2022).

[31] S. Yang and J.-B. Xu, “Density-wave-ordered phases of Rydberg atoms on a honeycomb lattice,” *Phys. Rev. E* **106**, 034121 (2022).

[32] T. Manovitz, S. H. Li, S. Ebadi, R. Samajdar, A. A. Geim, S. J. Evered, D. Bluvstein, H.-Y. Zhou, N. U. Koyluoglu, J. Feldmeier, P. E. Dolgirev, N. Maskara, M. Kalinowski, S. Sachdev, D. A. Huse, M. Greiner, V. Vuletic, and M. D. Lukin, “Quantum coarsening and collective dynamics on a programmable simulator,” *Nature* **638**, 86 (2025).

[33] S.-L. Zhu, “Scaling of Geometric Phases Close to the Quantum Phase Transition in the  $XY$  Spin Chain,” *Phys. Rev. Lett.* **96**, 077206 (2006).

[34] S.-S. Fu, X.-H. Li, and S.-L. Luo, “Detecting quantum phase transition via magic resource in the  $XY$  spin model,” *Phys. Rev. A* **106**, 062405 (2022).

[35] Z.-Y. Sun, Y.-Y. Wu, J. Xu, H.-L. Huang, B.-F. Zhan, B. Wang, and C.-B. Duan, “Characterization of quantum phase transition in the  $XY$  model with multipartite correlations and Bell-type inequalities,” *Phys. Rev. A* **89**, 022101 (2014).

[36] F.-W. Ma, S.-X. Liu, and X.-M. Kong, “Entanglement and quantum phase transition in the one-dimensional anisotropic  $XY$  model,” *Phys. Rev. A* **83**, 062309 (2011).

[37] R. Grazi, D. Sacco Shaikh, M. Sassetti, N. Traverso Ziani, and D. Ferraro, “Controlling energy storage crossing quantum phase transitions in an integrable spin quantum battery,” *Phys. Rev. Lett.* **133**, 197001 (2024).

[38] P. Nandi, S. Bhattacharyya, and S. Dasgupta, “Detection of quantum phase boundary at finite temperatures in integrable spin models,” *Phys. Rev. Lett.* **128**, 247201 (2022).

[39] F. Pázmárdi and Z. Dománski, “Quantum Phase Transitions in  $XY$  Spin Models,” *Phys. Rev. Lett.* **74**, 2363 (1995).

[40] S. Zamani, R. Jafari, and A. Langari, “Floquet dynamical quantum phase transition in the extended  $XY$  model: Nonadiabatic to adiabatic topological transition,” *Phys. Rev. B* **102**, 144306 (2020).

[41] S. Ghosh and A. Sen(De), “Dimensional enhancements in a quantum battery with imperfections,” *Phys. Rev. A* **105**, 022628 (2022).

[42] S. Ghosh, T. Chanda, S. Mal, and A. Sen(De), “Fast charging of a quantum battery assisted by noise,” *Phys. Rev. A* **104**, 032207 (2021).

[43] S. Satoori, S. Mahdavifar, and J. Vahedi, “Quantum correlations in the frustrated  $XY$  model on the honeycomb lattice,” *Sci. Rep.* **13**, 16034 (2023).

[44] S.-Y. Liu, Y.-R. Zhang, W.-L. Yang, and H. Fan, “Global quantum discord and quantum phase transition in  $XY$  model,” *Ann. Phys.* **362**, 805 (2015).

[45] G. A. P. Ribeiro and G. Rigolin, “Finite-temperature detection of quantum critical points: A comparative study,” *Phys. Rev. B* **109**, 245122 (2024).

[46] Z. Wang, A. Marandi, K. Wen, R. L. Byer, and Y. Yamamoto, “Coherent Ising machine based on degenerate optical parametric oscillators,” *Phys. Rev. A* **88**, 063853 (2013).

[47] Y. Inui and Y. Yamamoto, “Entanglement and quantum discord in optically coupled coherent Ising machines,” *Phys. Rev. A* **102**, 062419 (2020).

[48] K. Takata, A. Marandi, R. Hamerly, Y. Haribara, D. Maruo, S. Tamate, H. Sakaguchi, S. Utsunomiya, and Y. Yamamoto, “A 16-bit Coherent Ising Machine for One-Dimensional Ring and Cubic Graph Problems,” *Sci. Rep.* **6**, 34089 (2016).

[49] T. Inagaki, Y. Haribara, K. Igarashi, T. Sonobe, S. Tamate, T. Honjo, A. Marandi, P. L. McMahon, T. Umeiki, K. Enbutsu, O. Tadanaga, H. Takenouchi, K. Aihara, K.-I. Kawarabayashi, K. Inoue, S. Utsunomiya, and H. Takesue, “A coherent Ising machine for 2000-node optimization problems,” *Science* **354**, 603 (2016).

[50] P. L. McMahon, A. Marandi, Y. Haribara, R. Hamerly, C. Langrock, S. Tamate, T. Inagaki, H. Takesue, S. Utsunomiya, K. Aihara, R. L. Byer, M. M. Fejer, H. Mabuchi, and Y. Yamamoto, “A fully programmable 100-spin coherent Ising machine with all-to-all connections,” *Science* **354**, 614 (2016).

[51] N. Mwamsojo, F. Lehmann, K. Merghem, B.-E. Benkelfat, and Y. Frignac, “Optoelectronic coherent Ising machine for combinatorial optimization problems,” *Opt. Lett.* **48**, 2150 (2023).

[52] H. Takesue, K. Inaba, T. Honjo, Y. Yamada, T. Ikuta, Y. Yonezu, T. Inagaki, T. Umeiki, and R. Kasahara, “Finding independent sets in large-scale graphs with a coherent Ising machine,” *Sci. Adv.* **11**, eads7223 (2025).

[53] K. Inaba, Y. Yamada, and H. Takesue, “Thermodynamic quantities of two-dimensional Ising models obtained by noisy mean-field annealing and a coherent Ising machine,” *Phys. Rev. Appl.* **20**, 044074 (2023).

[54] T. Honjo, T. Sonobe, K. Inaba, T. Inagaki, T. Ikuta, Y. Yamada, T. Kazama, K. Enbutsu, T. Umeiki, R. Kasahara, K.-I. Kawarabayashi, and H. Takesue, “100,000-spin coherent Ising machine,” *Sci. Adv.* **7**, eabh0952 (2021).

[55] H. Takesue, Y. Yamada, K. Inaba, T. Ikuta, Y. Yonezu, T. Inagaki, T. Honjo, T. Kazama, K. Enbutsu, T. Umeiki, and R. Kasahara, “Observing a Phase Transition in a Coherent Ising Machine,” *Phys. Rev. Appl.* **19**, L031001 (2023).

[56] A. Yamamura, H. Mabuchi, and S. Ganguli, “Geometric Landscape Annealing as an Optimization Principle Underlying the Coherent Ising Machine,” *Phys. Rev. X* **14**, 031054 (2024).

[57] Y. Mizuno and T. Komatsuzaki, “Finding optimal pathways in chemical reaction networks using Ising machines,” *Phys. Rev. Res.* **6**, 013115 (2024).

[58] K. Terayama, M. Sumita, R. Tamura, and K. Tsuda, “Black-box optimization for automated discovery,” *Acc. Chem. Res.* **54**, 1334 (2021).

[59] D. B. Kell, “Scientific discovery as a combinatorial optimisation problem: how best to navigate the landscape of possible experiments?” *Bioessays* **34**, 236 (2012).

[60] M. O. Scully and M. S. Zubairy, *Quantum Optics* (Cambridge University Press, 1997).